

Single-Photon Detection Using Quantum Phase Transitions

Liping Yang¹ and Zubin Jacob¹

¹*Birk Nanotechnology Center and Purdue Quantum Center,
School of Electrical and Computer Engineering, Purdue University, West Lafayette, IN 47906, U.S.A.*

We propose a single-photon detector by exploiting the universal first-order quantum phase transition (QPT) in interacting spin systems. We utilize a time-dependent theoretical framework to study the absorption of a single photon pulse by an engineered defect (i.e., a nitrogen-vacancy center) which nucleates the single shot quantum measurement. The crucial step of amplifying the weak quantum signal occurs by coupling the defect to a system of interacting spins biased close to a QPT point. The macroscopic spin-order change during the QPT generates an amplified signal, which can be read out by a classical device. Our amplification scheme is based on the giant sensitivity of the first-order QPT, which fundamentally originates from the diverging higher-order spin-spin correlation at the phase transition point.

Utilizing the high sensitivity of thermodynamic (classical) phase transitions (TPTs) has a long and successful history for weak signal detection, such as the Wilson cloud chamber [1] and the bubble chamber [2]. One recent prominent example is the superconducting nanowire single-photon detector (SNSPD) [3], which has achieved the state-of-art of quantum efficiency, timing jitter and dark counting rate in single-photon detection [4]. The defects in the superconductor absorb the incident single-photon pulse (SPP) nucleating a hotspot, which diffuses and finally breaks the superconductivity of the nanowire to generate an amplified signal. The essential amplification mechanism relies on the concept of a optimum critical bias to ensure that even an SPP can trigger a phase transition from the superconducting to the normal domain.

In this letter, we propose a practical design for a single photon detector that exploits a quantum phase transition (QPT) in the amplification step. We utilize a time-dependent theoretical framework of QPTs to study single photon pulses interacting with a defect within a macroscopic system of interacting spins. We show that even a single photon level perturbation to a system of interacting spins can change the long-range order leading to a single shot quantum measurement. This amplification scheme necessarily requires the detector to be biased closed to the phase transition point. We also show that the giant sensitivity of the first-order QPTs fundamentally originates from the diverging higher-order correlation at the phase transition point. Our detector is a quantum analog of the SNSPD which exploits the superconducting phase transition for single photon detection.

This paper builds on our recent proposal of the quantum critical detector (QCD) that functions by a weak signal triggering a first-order QPT [5, 6]. We note however, that it is still a fundamental open question whether a single photon perturbation can trigger the QPT which is the focus of this work. In contrast with TPTs, QPTs occur at zero temperature and can be triggered even by varying a physical parameter [7], such as magnetic field or interaction strength. Consequently, the quantum fluctuations, arising from Heisenberg's uncertainty principle, dominate and drive the transition to realize the amplification of the quantum signal. Thus, our detector can have higher signal-to-noise ratio and lower dark counting rate than

detectors utilizing TPTs.

The proposed detector is fundamentally different from the quantum interferometers for parameter estimation or quantum sensing/metrology [8–10] (see Table I). The enhanced sensitivity in quantum interferometers benefits from the accumulated phase from a large number of synchronized non-interacting particles in repeated measurements [11–13]. In stark contrast, the giant sensitivity in our scheme originates from the singular behavior of strongly correlated systems at the phase transition point [5, 6]. The detection events in the presented scheme are single-shot measurements. Our approach is also distinct from the well-established quantum linear amplifiers [14, 15]. The gain of linear quantum amplifiers arises from the coherent pumping in the ancillary modes. Simultaneously, phase information is encoded in the quadratures of the signal modes which is preserved during the amplification. However, the quantum gain of our device results from the macroscopic change in the order parameter during the QPT. The phase information in the input signal (e.g., the pulse shape) is lost during the amplification and only the pulse number information (0 or 1) is read out by the amplifier. Thus the behavior of our detector is closer to single photon avalanche diodes (SPADs) and SNSPDs.

Single-photon detection—We now discuss the working mechanism and implementation of the QCD for SPP detection. The first step of the detection event is the transduction (absorption) of the incident single photon in an engineered defect. This process is similar to the generation of the first electron-hole pair in single-photon avalanche diode or the first photo-emission event in the photo-multiplier tube. The highly efficient transduction is realized via a Λ -structure transition as shown in Fig 1. In contrast to a two-level absorber, this Λ -transition defect has three main benefits: (1) higher absorption probability [16, 17]; (2) longer lifetime of the destination state $|e\rangle$ [18] conducive for efficient read-out; (3) connection of the optical transition in the absorber and the RF-frequency dynamics in the amplifier. One promising example of such kind of absorber is a nitrogen-vacancy (NV) center. The states $|g\rangle$ and $|e\rangle$ correspond to the two ground spin states $|0\rangle$ and $|+1\rangle$ of the NV. The T_1 time (lifetime of the state $|e\rangle = |+1\rangle$) of NV centers is few milliseconds at room temperature and even much longer at lower temperatures [19]. The Λ transition can

Quantum Interferometers for Metrology/Sensing	Quantum Counters for Single-Photon Detection
Phase interference based	Not an interference measurement; Non-adiabatic transitions dominated dynamics
Repeative measurements	Single-shot measurement
Slope of the continuous transition determines the sensitivity	Discontinuity leads to clicks
No concept of timing jitter and dark counting rate	High counting rate and low dark counting rate is required
NOON (GHZ) state to reach the Heisenberg limit in a Mach-Zehnder (Ramsey) Interferometer [8]	Single-photon avalanche diode; superconducting nanowire single-photon detectors

TABLE I. Contrast between single-photon detection (quantum counters) and quantum metrology (sensing).

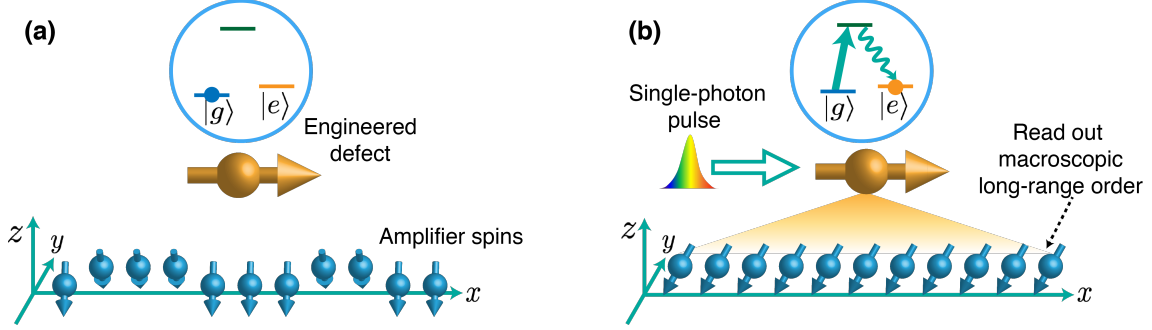


FIG. 1. Single photon detection via quantum phase transition (QPT). The interacting spins at the bottom, which function as the amplifier of the detector, are critically biased close to the first-order QPT point. The three states in the absorber on the top form a Λ -structure. After absorption of a single-photon pulse, the absorber is excited from the ground state $|g\rangle$ and finally relaxes to the meta-stable state $|e\rangle$. After the $|g\rangle \rightarrow |e\rangle$ transition, the absorber exerts an effective magnetic field on the amplifier spins. This magnetic field triggers a QPT in the spins underneath. Initially, the spins are polarized in the yz -plane (see panel a). After the phase transition, the spins rotate to the xz -plane (see panel b). This macroscopic spin-order change functions as the output signal of the single-photon detector.

be realized with the spin non-conserving transition [20] (see the supplementary material [21]). After the transduction, the information of the SPP is written in the $|e\rangle$ state of the absorber.

The second principle is effective engineering of the absorber-amplifier interaction to guarantee that the absorbed energy is transferred to the readout channel to trigger the QPT. In our detector, the coupling between the absorber and the amplifier is engineered in x -direction

$$\hat{H}_{\text{int}} = B_x |e\rangle \langle e| \sum_j \hat{\sigma}_j^x. \quad (1)$$

This dispersive coupling with strength B_x acts an effective magnetic field for the amplifier spins. As shown in the following, the defect functions as a control of the QPT in the amplifier. More importantly, the dispersive coupling avoids additional decoherence of the amplifier induced by the SPP. The NV center couples to its surrounding spins dispersively as in equation (1) when the strength B_x is much smaller the ground-state zero-field splitting $\Delta_{\text{gs}} \approx 2.87$ GHz [22].

The essential step of an SPP detection is the amplification, since the excitation in the defect after the transduction is still an extremely weak quantum signal. In our detector, the amplification is realized by exploiting the giant sensitivity of the first-order QPT. With the mean-field theory, we predicted a

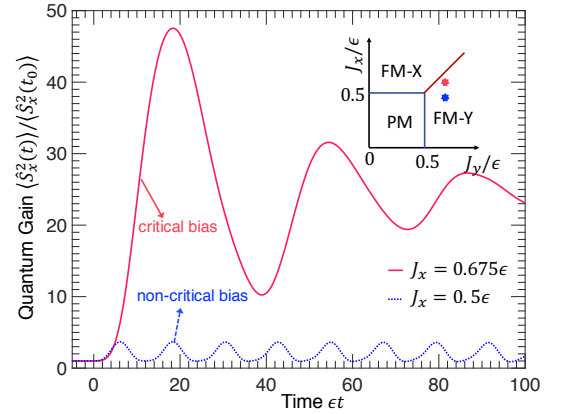


FIG. 2. Single-photon pulse induced first-order QPT. After absorption of a single-photon pulse, the absorber is flipped to the state $|e\rangle$, on which the absorber exerts a weak magnetic field $B_x \times P_e(t)$ ($P_e(t)$ the population of the state $|e\rangle$) on the amplifier with $N = 400$ spins. Only if the the amplifier is optically biased around the critical point $J_{x,c} \equiv J_y$, the time varying field can trigger a first-order QPT to obtain a large quantum gain. Here, the spin-spin coupling in the y -direction is fixed at $J_y = 0.7$ and the absorber-amplifier coupling $B_x = 0.01\epsilon$.

universal first-order QPT in interacting spin systems [6]

$$\hat{H}_{\text{Am}} = \frac{1}{2}\epsilon \sum_{j=1}^N \hat{\sigma}_j^z - \frac{1}{n} \sum_{\langle i < j \rangle} (J_x \hat{\sigma}_i^x \hat{\sigma}_j^x + J_y \hat{\sigma}_i^y \hat{\sigma}_j^y), \quad (2)$$

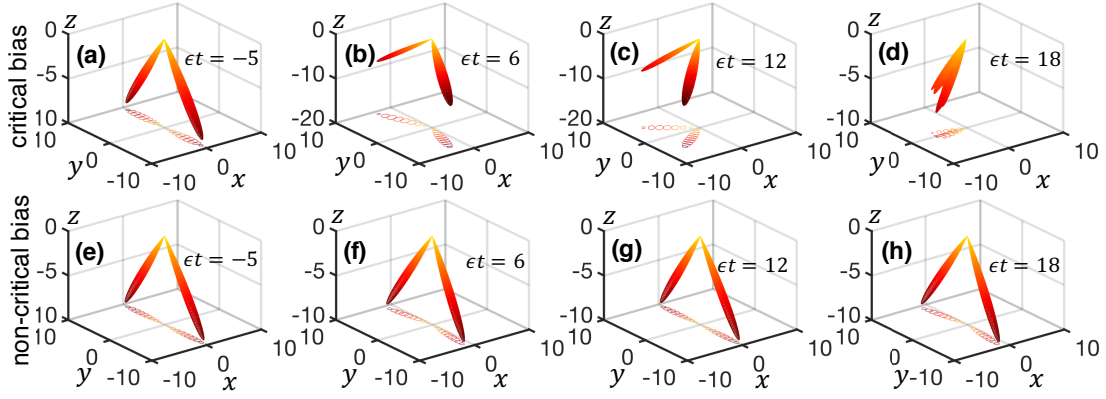


FIG. 3. Dynamics of the amplifier. The spin Q -function characterizes the polarization distribution of the amplifiers spins. The first rows (a-d) shows the dynamic change in the Q -function with bias $J_x = 0.675\epsilon$ very close to the phase transition point $J_{x,c} = J_y = 0.7\epsilon$. The second row (e-h) is for the case with $J_x = 0.5\epsilon$ far from $J_{x,c}$. The curves underneath are the contour projections of the corresponding Q -functions in xy -plane.

where ϵ is the energy splitting of the spins along z direction, J_x and J_y are the strengths of the ferromagnetic spin-spin couplings in x - and y -direction respectively, and $\hat{\sigma}_j^\alpha$ ($\alpha = x, y, z$) are the Pauli matrices of the j th spin. The summation $\langle i < j \rangle$ runs over n coupled neighbours. For the 1-dimensional Ising chain with $n = 1$, the short-range coupling only exists between the nearest neighbours [7]. For the Lipkin-Meshkov-Glick (LMG) model with $n = N - 1$ (N the total spin number) [23], all the spins are coupled with each other. The interacting spins function as the amplifier of our proposed SPP counter.

The amplifier has two ferromagnetic (FM) phases: FM-X and FM-Y with long-range spin order in x - and y -direction. The competition between these two FM phases results in the first-order QPT, which exhibits giant sensitivity for weak signal detection [6]. The quantum phases and the corresponding QPTs can be characterized by two magnetic order parameters

$$\zeta_x \equiv \langle \hat{S}_x^2 \rangle_0 / N^2 \text{ and } \zeta_y \equiv \langle \hat{S}_y^2 \rangle_0 / N^2, \quad (3)$$

which describe the magnetic fluctuations in the xy -plane. Here, $\hat{S}_\alpha = \sum_j \hat{\sigma}_j^\alpha / 2$ are the collective spin operators and $\langle \dots \rangle_0$ means average on the ground-state of the amplifier. The second-order QPTs in interacting spin systems have been extensively demonstrated in recently experiments [24–26]. Specifically, the second-order QPT in the LMG model (with long-range spin-spin coupling only in x -axis) has also been demonstrated in a recent experiment with 16 Dysprosium atoms [27]. We suggest that by adding an additional laser to induce the long-range coupling in y -direction, the first-order QPT due to the competition between the two FM phases can also be observed. This provides a promising platform to build a single-photon detector utilizing first-order QPT in the LMG model. In the following, we numerically demonstrate the detection of SPPs with such a QCD. The first-order QPT in the LMG amplifier occurs at $J_x = J_y > \epsilon/2$ [6].

The amplification and single-shot readout of the quantum information stored in the state $|e\rangle$ is realized by exploiting the first-order QPT in the amplifier. Initially, the spin-spin cou-

pling J_x is pre-biased slightly below the phase transition point $J_{x,c} \equiv J_y$ and the amplifier is initialized in its ground state of the FM-Y phase. After absorption of a SPP pulse, the absorber is flipped to the state $|e\rangle$ with probability $P_e(t)$ [21]. Thus, the additional effective magnetic field experienced by the amplifier spins is $B_x \times P_e(t)$. The initial critical bias guarantees that the small magnetic field perturbation $B_x \times P_e(t)$ from the absorber can trigger a QPT and leads to efficient amplification.

There are two ways to read out the amplified signal in practice. One is to directly measure the spontaneous magnetization $\sqrt{\zeta_x}$ of the amplifier in x -direction, which increases from an extremely small value to a finite value after the collective rotation of the spins. Another option is to couple the amplifier spin with a cavity as proposed in our previous works [5, 6]. The energy prestored in the spins is transferred to the cavity mode generating macroscopic excitations after the QPT. The photons leak out from cavity can be directly measured with classical photodetectors.

To characterize the detection sensitivity, we define the quantum gain of the amplifier as

$$G(t) = \langle \hat{S}_x^2(t) \rangle / \langle \hat{S}_x^2(t_0) \rangle. \quad (4)$$

We contrast the time-dependent quantum gain for the cases of critical bias (the red-solid curve) and non-critical bias (the blue dotted curve) in Fig. 2. In the subgraph, we present the schematic of the first-order QPT boundary (the red curve) in the phase diagram. The two starts mark out the the positions of these two biases. It is clearly seen that the efficient amplification can only be obtained if the system is optimally biased close to the phase transition point [5].

To reveal the intrinsic change within the amplifier, we contrast the time-dependent spin Q -function of the amplifier for different biases in Fig. 3. The first row (a-d) and the second row (e-h) correspond to critical and non-critical bias cases, respectively. In both cases, the amplifier starts from the FM-Y phase with spins polarized in the yz -plane. The two arms of the Q -function in the yz -plane at time $t_0 = -5/\epsilon$ (the time

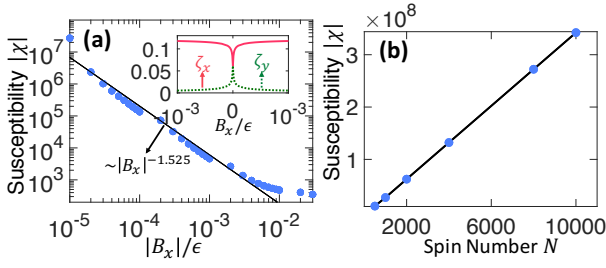


FIG. 4. Singular behavior in the susceptibility. (a) The susceptibility χ diverges at the phase transition point $J_x = J_y = 0.7\epsilon$. The subgraph shows the abrupt changes in the order parameters in the first-order QPT transition with spin number $N = 1000$. (b) The susceptibility χ near the phase transition point increases linearly with the spin number N . Here, the perturbation magnetic field is set as $B_x = 10^{-5}\epsilon$.

before the absorption of the pulse) correspond to the two degenerate ground states of the FM-Y phase [6]. For the first row, the incident SPP triggers a phase transition to the FM-X phase. The spins rotate 90° to the xz -plane at time $t_0 = 18/\epsilon$ in Fig. 3 (d). This reveals the dynamic change in the long-range spin order within the amplifier and clearly shows the signature of the detection event. In contrast, no macroscopic spin order change occurs when the amplifier is biased far from the phase transition point. The polarization of the spins marginally varies with time in Fig. 3 (e-h).

Our simulation of the amplifier dynamics has ignored the decoherence of the interacting spins that may degrade the performance of a realistic device. However, the amplification has completed within the time $\epsilon T_{\text{Am}} \approx 15$ [21], which is usually much shorter than the decoherence time of the spins. If the amplifier is composed of electron spins with typical energy splitting $\epsilon \sim 1$ GHz and coherence time $T_2^* \sim 1\mu\text{s}$ [28], we have $\epsilon T_2^* \approx 1000 \gg \epsilon T_{\text{Am}}$. For nuclear spins with typical energy splitting 1 MHz and coherence time $T_2^* \sim 1$ ms [29], the decoherence time is still much longer than the amplification time. With dynamical decoupling techniques [30, 31], the coherence time of the spins can be further prolonged 2–3 orders of magnitude [32–34], which is far more than the required time for amplification. The dipole-dipole interaction between the NV center and nuclear spins at the typical distance 1 nm is around 20 kHz. This effective magnetic field ($B_x/\epsilon \approx 0.02$) is large enough to trigger the QPT.

The critical scaling of the detector— The giant sensitivity of the detector fundamentally originates from the singular behaviors of the system at the phase transition point. We now show the singular scalings of the amplifier. We also notice that in most cases, it is difficult for weak input signals to change the coupling strength within the amplifier [5]. Here, we show that a weak magnetic field perturbation can also break the balance of the two FM phase at the phase boundary $J_x = J_y$ to trigger the first-order QPT. This also lays the foundation of the amplification mechanism in our proposed single-photon detector. As shown in the subgraph of Fig. 4 (a), the order parameter ζ_x increases swiftly with the perturbation magnetic

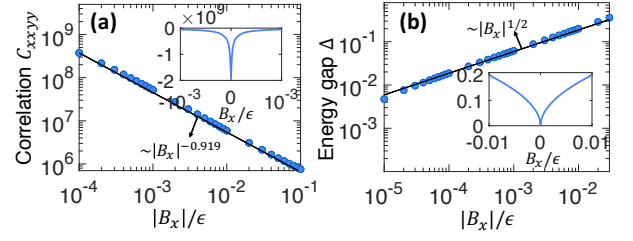


FIG. 5. Singular behavior of the higher-order correlation and energy gap. **a** The higher-order correlation C_{xxyy} diverges at the phase transition point $J_x = J_y = 0.7\epsilon$. **b** The energy gap vanishes at the phase transition point. The subgraphs show the same curves in the linear coordinates. Both curves are symmetric on the two sides of the phase transition. The solid black lines are the algebraic fittings. The spin number is set as $N = 1000$.

field in x -direction and the other order parameter ζ_y drops. The sensitivity to the magnetic field is characterized by the susceptibility of the spontaneous magnetization

$$\chi = \left. \frac{d\sqrt{\zeta_x}}{dB_x} \right|_{B_x \rightarrow 0} \propto |B_x|^{-\gamma}, \quad (5)$$

which is symmetric on the two sides of the transition with singular exponent $\gamma \approx 1.525$. The same susceptibility for the spontaneous magnetization $\sqrt{\zeta_y}$ with respect to a magnetic field in y -axis can also be obtained (data not shown). The susceptibility diverges linearly with the spin number $\chi \sim N$ as shown in Fig. 4 (b).

We emphasize that in first-order QPTs, a singularity occurs on the higher-order magnetic correlation. This is fundamentally different from the traditional TPTs, in which the diverging spatial correlation length ξ in the microscopic correlator $\langle (\hat{\sigma}_i^x - \langle \hat{\sigma}_i^x \rangle) (\hat{\sigma}_{i+\xi}^x - \langle \hat{\sigma}_{i+\xi}^x \rangle) \rangle$ leads to the divergence of the magnetic susceptibility [35]. However, in the LMG model, the spins are all coupled with each other with homogeneous strength and the spins are indistinguishable. Thus, we cannot define a simple correlation length ξ for the LMG model. Alternatively, we define a higher-order correlation function

$$C_{xxyy} = \frac{1}{2} \langle \hat{S}_x^2 \hat{S}_y^2 + \hat{S}_y^2 \hat{S}_x^2 \rangle_0 - \langle \hat{S}_x^2 \rangle_0 \langle \hat{S}_y^2 \rangle_0 \propto |B_x|^{-\tilde{\nu}}, \quad (6)$$

to characterize the macroscopic correlation between the magnetic fluctuations in x - and y - axis.

The diverging C_{xxyy} in the subgraph of Fig. 5 (a) shows the strong negative correlation between \hat{S}_x^2 and \hat{S}_y^2 at the phase transition point. The negative correlation reveals the fact that the order parameter ζ_y decreases as the other one ζ_x increases. The corresponding singular exponent is $\tilde{\nu} \approx 0.919$ as shown by the black fitting curve. This exponent is universal for the LMG model, as it is independent on the spin number N as well as the position on the first-order QPT boundary in Fig. 2 [21]. We note that $\tilde{\nu}$ is similar to the traditional correlation length critical exponent [35, 36]. We also find that the lower-order correlation $(1/2) \langle \hat{S}_x \hat{S}_y + \hat{S}_y \hat{S}_x \rangle_0 - \langle \hat{S}_x \rangle_0 \langle \hat{S}_y \rangle_0$ shows no singularity [21].

Another typical character of QPTs is that the energy gap Δ vanishes at the phase transition point as shown in Fig. 5b. The corresponding exponent is given by $\Delta \sim |B_x|^{1/2}$, which is same as the second-order QPT in LMG model [37–39]. Previous study on the size scaling for the LMG model shows that energy gap Δ also vanishes with the increasing spin number $\Delta \sim 1/N$ at the phase transition point [40, 41].

Discussion—Our work provides a practical framework for single photon pulse detection using QPTs. This defect-controlled-QPT device is based on the fact that the first-order QPT in interaction spin systems can be induced by a weak in-plane magnetic field. Our theoretical proposal can be directly implemented in current QPT simulators [24–26]. We note that for microscopic systems, zero temperature generally implies preparing a system in a pure quantum (ground) state.

This work is supported by the DARPA DETECT ARO award (W911NF-18-1-0074).

-
- [1] N. N. D. Gupta and S. K. Ghosh, *Rev. Mod. Phys.* **18**, 225 (1946).
- [2] D. A. Glaser, *Phys. Rev.* **87**, 665 (1952).
- [3] G. Goltzman, O. Okunev, G. Chulkova, A. Lipatov, A. Semenov, K. Smirnov, B. Voronov, A. Dzardanov, C. Williams, and R. Sobolewski, *Applied physics letters* **79**, 705 (2001).
- [4] M. D. Eisaman, J. Fan, A. Migdall, and S. V. Polyakov, *Review of scientific instruments* **82**, 071101 (2011).
- [5] L.-P. Yang and Z. Jacob, *Optics express* **27**, 10482 (2019).
- [6] L.-P. Yang and Z. Jacob, *arXiv preprint arXiv:1905.07420* (2019).
- [7] S. Sachdev, *Quantum phase transitions* (Wiley Online Library, 2007).
- [8] V. Giovannetti, S. Lloyd, and L. Maccone, *Science* **306**, 1330 (2004).
- [9] V. Giovannetti, S. Lloyd, and L. Maccone, *Physical review letters* **96**, 010401 (2006).
- [10] C. L. Degen, F. Reinhard, and P. Cappellaro, *Rev. Mod. Phys.* **89**, 035002 (2017).
- [11] B. Yurke, S. L. McCall, and J. R. Klauder, *Phys. Rev. A* **33**, 4033 (1986).
- [12] J. P. Dowling, *Phys. Rev. A* **57**, 4736 (1998).
- [13] J. J. Bollinger, W. M. Itano, D. J. Wineland, and D. J. Heinzen, *Phys. Rev. A* **54**, R4649 (1996).
- [14] C. M. Caves, *Physical Review D* **26**, 1817 (1982).
- [15] N. Bergeal, R. Vijay, V. Manucharyan, I. Siddiqi, R. Schoelkopf, S. Girvin, and M. Devoret, *Nature Physics* **6**, 296 (2010).
- [16] S. M. Young, M. Sarovar, and F. m. c. Léonard, *Phys. Rev. A* **97**, 033836 (2018).
- [17] Y. Wang, J. c. v. Minář, L. Sheridan, and V. Scarani, *Phys. Rev. A* **83**, 063842 (2011).
- [18] L.-P. Yang, H. X. Tang, and Z. Jacob, *Phys. Rev. A* **97**, 013833 (2018).
- [19] A. Jarmola, V. M. Acosta, K. Jensen, S. Chemerisov, and D. Budker, *Phys. Rev. Lett.* **108**, 197601 (2012).
- [20] Y. Chu, M. Markham, D. J. Twitchen, and M. D. Lukin, *Phys. Rev. A* **91**, 021801 (2015).
- [21] See Supplemental Material for information about the details of single-photon transduction and higher-order correlations of amplifier spins.
- [22] N. Zhao, J.-L. Hu, S.-W. Ho, J. T. Wan, and R. Liu, *Nature nanotechnology* **6**, 242 (2011).
- [23] H. J. Lipkin, N. Meshkov, and A. Glick, *Nuclear Physics* **62**, 188 (1965).
- [24] J. Zhang, G. Pagano, P. W. Hess, A. Kyprianidis, P. Becker, H. Kaplan, A. V. Gorshkov, Z.-X. Gong, and C. Monroe, *Nature* **551**, 601 (2017).
- [25] H. Bernien, S. Schwartz, A. Keesling, H. Levine, A. Omran, H. Pichler, S. Choi, A. S. Zibrov, M. Endres, M. Greiner, *et al.*, *Nature* **551**, 579 (2017).
- [26] Harris *et al.*, *Science* **361**, 162 (2018).
- [27] V. Makhlov, T. Satoor, A. Evrard, T. Chalopin, R. Lopes, and S. Nascimbene, *arXiv preprint arXiv:1905.00807* (2019).
- [28] C. A. Ryan, J. S. Hodges, and D. G. Cory, *Phys. Rev. Lett.* **105**, 200402 (2010).
- [29] B. Smeltzer, J. McIntyre, and L. Childress, *Phys. Rev. A* **80**, 050302 (2009).
- [30] N. Zhao, S.-W. Ho, and R.-B. Liu, *Phys. Rev. B* **85**, 115303 (2012).
- [31] W. Yang, W.-L. Ma, and R.-B. Liu, *Reports on Progress in Physics* **80**, 016001 (2016).
- [32] G. Balasubramanian, P. Neumann, D. Twitchen, M. Markham, R. Kolesov, N. Mizuochi, J. Isoya, J. Achard, J. Beck, J. Tissler, *et al.*, *Nature materials* **8**, 383 (2009).
- [33] T. D. Ladd, D. Maryenko, Y. Yamamoto, E. Abe, and K. M. Itoh, *Phys. Rev. B* **71**, 014401 (2005).
- [34] P. C. Maurer, G. Kucsko, C. Latta, L. Jiang, N. Y. Yao, S. D. Bennett, F. Pastawski, D. Hunger, N. Chisholm, M. Markham, *et al.*, *Science* **336**, 1283 (2012).
- [35] M. Kardar, *Statistical physics of fields* (Cambridge University Press, 2007), Chap. 1.
- [36] J. Dziarmaga, *Advances in Physics* **59**, 1063 (2010).
- [37] N. Defenu, T. Enss, M. Kastner, and G. Morigi, *Phys. Rev. Lett.* **121**, 240403 (2018).
- [38] M. Xue, S. Yin, and L. You, *Phys. Rev. A* **98**, 013619 (2018).
- [39] P. Ribeiro, J. Vidal, and R. Mosseri, *Phys. Rev. E* **78**, 021106 (2008).
- [40] R. Botet and R. Jullien, *Phys. Rev. B* **28**, 3955 (1983).
- [41] S. Dusuel and J. Vidal, *Phys. Rev. B* **71**, 224420 (2005).

Supplementary Material for: “Single photon detection using quantum phase transitions”

Liping Yang¹ and Zubin Jacob^{1,*}

¹*Birck Nanotechnology Center and Purdue Quantum Center,
School of Electrical and Computer Engineering, Purdue University, West Lafayette, IN 47906, U.S.A.*

I. Λ -TRANSDUCTION IN NV CENTER

Usually, the optical transition in nitrogen-vacancy (NV) center does not change the state of the spin degree of freedom. Thus, a single-photon pulse (SPP) cannot induced a Λ -type transition to realize the flip of the two ground spin states $|0\rangle \rightarrow |1\rangle$ in an NV center. To solve this problem, we need to construct a spin non-conservation transition in NV. One approach is combining a linearly polarized laser with an additional circularly polarized laser, which has been demonstrated to realized all-optical control of the NV ground-state spin [1]. Here, we use another method by utilizing the energy crossing in the excited states of the NV as shown in Fig. 1. We add strain to the NV at the energy crossing point of the two excited states $|E_y\rangle = |a_1 e_y - e_y a_1\rangle \otimes |0\rangle$ and $|E_1\rangle = |E_-\rangle \otimes |-1\rangle - |E_+\rangle \otimes |+1\rangle$ (with $E_{\pm} = a_1 e_{\pm} - e_{\pm} a_1$ and $e_{\pm} = \mp(e_x \pm i e_y)$) [2]. Here, $\{|a_1\rangle, |e_x\rangle, |e_y\rangle\}$ and $\{|-1\rangle, |0\rangle, |+1\rangle\}$ are the orbital basis of the excited states and the triplet spin states (the two-hole representation). The coupling Δ'' between $|E_y\rangle$ and $|E_1\rangle$ realizes the spin non-conservation transition. Now, the effective Hamiltonian for the NV reads

$$\hat{H}_{\text{NV}} = \Delta_{\text{gs}} |1\rangle \langle 1| + \omega_y |E_y\rangle \langle E_y| + \omega_1 |E_1\rangle \langle E_1| + \Delta''(|E_y\rangle \langle E_1| + |E_1\rangle \langle E_y|), \quad (1)$$

where the energy of the ground spin state $|0\rangle$ is set as zero, $\Delta_{\text{gs}} \approx 2.87$ GHz the zero-field splitting between ground spin states, and $\omega_y = \omega_1$ (the strain has been taken into account) are the energy difference between the two excited states and the ground state $|0\rangle$.

The interaction between the NV and the incident SPP is given by

$$\hat{H}_{\text{pump}} = i\hbar \int_0^{\infty} d\omega [g(\omega) e^{i\vec{k}\cdot\vec{r}_{\text{NV}}} \hat{a}(\omega) |E_y\rangle \langle 0| - \text{h.c.}], \quad (2)$$

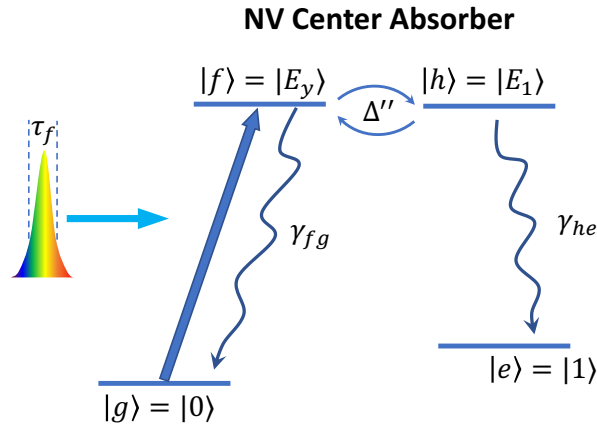


Figure 1. Single-photon transduction (absorption) process. The incident single-photon pulse excited the NV center to the excited state $|f\rangle = |E_y\rangle$. Via the spin non-conservation coupling Δ'' between states $|E_y\rangle$ and $|h\rangle = |E_1\rangle$, this excitation can be transferred to the ground spin state $|e\rangle = |1\rangle$ after the spontaneous decay. To realize an efficient transduction, the bandwidth matching between pulse length τ_f , the spontaneous decay rates γ_{fg} and γ_{he} , and the coupling strength Δ'' must be carefully considered (see follow).

* zjacob@purdue.edu

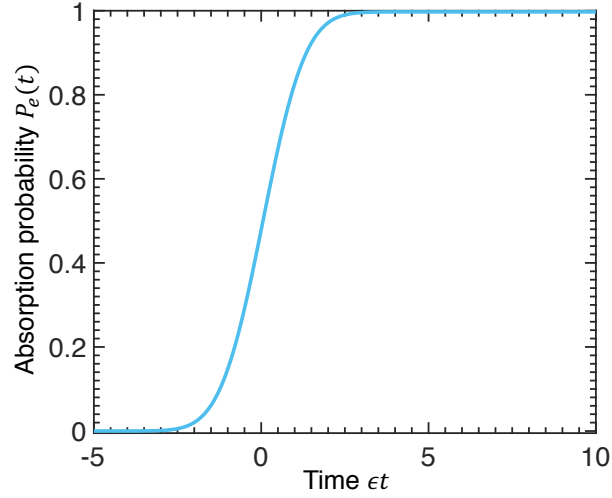


Figure 2. **Time-dependent absorption probability.** The length of the Gaussian pulse is set as $\epsilon\tau_f = 1$. The coupling between the two excited state $|f\rangle$ and $|h\rangle$ is $\Lambda'' = 5\epsilon$ and the spontaneous decay rates of these two excited states are $\gamma_{fg} = \gamma_{he} = \Gamma = 10\epsilon$.

where $\hat{a}(\omega)$ is the bosonic operator of the pulse mode with frequency $\omega = c|\vec{k}|$, \vec{r}_{NV} is the position of the NV center, and the rotating-wave approximation has been taken. The amplitude of the NV-SPP interaction spectrum is given by

$$g(\omega) = \sqrt{\frac{\omega}{4\pi\epsilon_0\hbar c\mathcal{A}}}(\vec{\epsilon} \cdot \vec{d}_{0y}),$$

where \mathcal{A} is the effective transverse cross section of the pulse [3], \vec{d}_{0y} the electric dipole vector of the $|0\rangle \rightarrow |E_y\rangle$ transition, and the unit vector $\vec{\epsilon}$ denotes the polarization of the pulse. The wave-packet amplitude of a Gaussian SPP is given by

$$\xi(t) = \left(\frac{1}{2\pi\tau_f^2}\right)^{1/4} \exp\left[-\frac{t^2}{4\tau_f^2} - i\omega_0 t\right], \quad (3)$$

with center frequency ω_0 and pulse length τ_f [3]. The incident SPP pulse is resonant with $|0\rangle \rightarrow |E_y\rangle$ transition, i.e., $\omega_0 = \omega_y = \omega_1$.

We note that the excited state $|E_1\rangle$ is a superposition of states with spin $| -1\rangle$ and $| +1\rangle$. After the spontaneous decay, a quantum entanglement state $|\psi\rangle = (|\sigma_-| -1\rangle - |\sigma_+| +1\rangle)$ between a outgoing circularly polarized single photon and the ground spin states of the NV is obtained [4]. The amplifier performs a projection measurement on the spin state of the NV. Each time, only one of the spin states can be detected. Actually, both of the ground spin states $|\pm 1\rangle$ can provide an effective magnetic field (with inverse direction) for amplifier spins to trigger the quantum phase transition. If the coherence of the NV center has been preserved during the amplification process, the detector will finally go to a NV-amplifier entangled state, i.e., $(| +1\rangle \otimes | -M_x\rangle + | -1\rangle \otimes | M_x\rangle)/\sqrt{2}$ ($| \pm M_x\rangle$ are the excited states of the amplifier with positive and negative spontaneous magnetization in x -axis, respectively). Here, without loss of generality, we only take the case that the NV decays to the ground spin state $|1\rangle$ as an example. For simplicity, we use the following denotation hereafter

$$|0\rangle = |g\rangle \quad (4)$$

$$|1\rangle = |e\rangle \quad (5)$$

$$|E_y\rangle = |f\rangle \quad (6)$$

$$|E_1\rangle = |h\rangle \quad (7)$$

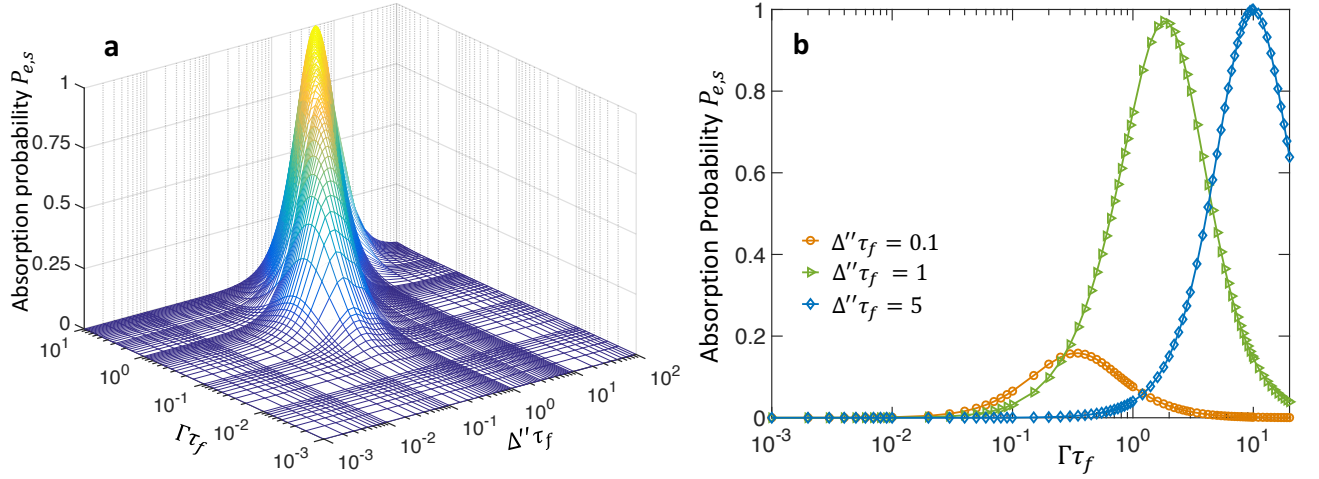


Figure 3. **Optimization of the transduction probability.** **a** The steady-state (the max) value $P_{e,s}$ of the population of the state $|e\rangle$ as a function of Δ'' and Γ is shown. Here, Δ'' is the coupling between the two excited states $|f\rangle$ and $|h\rangle$. The two spontaneous decay rates are set to be the same $\gamma_{fg} = \gamma_{he} = \Gamma$. The pulse length is set as $\tau_f\epsilon = 1$. **b** The steady-state probabilities $P_{e,s}$ for specific couplings Δ'' are given.

II. DYNAMICS OF SINGLE-PHOTON DETECTIONS

The full dynamics of the detector under the pumping of the center spin by a single-photon pulse is given by a time-dependent master equation [5, 6]

$$\frac{d}{dt}\rho_{\text{tot}}(t) = -i[\hat{H}, \rho_{\text{tot}}(t)] + \mathcal{L}_P(t)\rho_{\text{tot}}(t) + \mathcal{L}_{\text{SD}}\rho_{\text{tot}}(t). \quad (8)$$

Here, $\hat{H} = \hat{H}_{\text{NV}} + \hat{H}_{\text{Am}} + \hat{H}_{\text{int}}$ is the total Hamiltonian of the detector. The Hamiltonian of the NV is given in equation (1). The amplifier is described by the Lipkin-Meshkov-Glick (LMG) model [7–9],

$$\hat{H}_{\text{Am}} = \frac{1}{2}\epsilon \sum_{j=1}^N \hat{\sigma}_j^z - \frac{1}{N} \sum_{i<j} (J_x \hat{\sigma}_i^x \hat{\sigma}_j^x + J_y \hat{\sigma}_i^y \hat{\sigma}_j^y) \quad (9)$$

with energy splitting ϵ in z -direction and the homogeneous long-range couplings J_x and J_y in xy -plane. The interaction between the NV absorber and the amplifier spins is described by

$$\hat{H}_{\text{int}} = B_x |e\rangle \langle e| \sum_j \hat{\sigma}_j^x. \quad (10)$$

The initial density matrix $\rho_{\text{tot}}(t_0) = I_p \otimes \rho_{\text{NV}}(t_0) \otimes \rho_{\text{Am}}(t_0)$ of the whole system is composed of three parts: (1) I_p is the 2×2 identity matrix for a n -photon Fock-state pulse; (2) $\rho_{\text{NV}}(t_0) = |g\rangle \langle g|$ for the ground-state NV center; (3) $\rho_{\text{Am}}(t_0)$ the ground-state of H_{Am} with specifically engineered bias couplings J_x and J_y .

The pumping from a quantum pulse is given by

$$\mathcal{L}_P \rho_{\text{tot}} = \sqrt{\gamma_{fg}\eta} \{ \xi(t-t_0) e^{i\phi} [\hat{\tau}_+ \rho_{\text{tot}} \hat{\sigma}_{fg}] + \xi^*(t-t_0) e^{-i\phi} [\hat{\sigma}_{gf} \rho_{\text{tot}} \hat{\tau}_-] \}, \quad (11)$$

with the spontaneous decay rate γ_{fg} from the excited state $|f\rangle$ back to the ground state $|g\rangle$ and ladder operators $\hat{\sigma}_{fg} = |f\rangle \langle g|$ and $\hat{\sigma}_{gf} = |g\rangle \langle f|$. Here, η_j characterizes the scattering efficiency of the NV, $\phi = \vec{k}_0 \cdot \vec{r}_{\text{NV}}$ ($\omega_0 = c|\vec{k}_0|$), t_0 is the propagating time for pulse to arrive at the NV center, and the time-dependent wave-packet amplitude $\xi(t)$ of the Fock-state pulse is given in equation (3). The raising operator $(\hat{\tau}_-)^{\dagger} = \hat{\tau}_+ = \begin{bmatrix} 0 & 1 \\ 1 & 0 \end{bmatrix}$ couples the different photon-number subspace for Fock-state pulse.

As usually the coherence time of the amplifier is much longer than amplification time, we only consider the decay of the center spin from the electronic excited state

$$\mathcal{L}_{\text{SD}} \rho_{\text{tot}} = \gamma_{fg} [\hat{\sigma}_{gf} \rho_{\text{tot}} \hat{\sigma}_{fg} - \frac{1}{2} \hat{\sigma}_{fg} \hat{\sigma}_{gf} \rho_{\text{tot}} - \frac{1}{2} \rho_{\text{tot}} \hat{\sigma}_{fg} \hat{\sigma}_{gf}] + \gamma_{he} [\hat{\sigma}_{eh} \rho_{\text{tot}} \hat{\sigma}_{he} - \frac{1}{2} \hat{\sigma}_{he} \hat{\sigma}_{eh} \rho_{\text{tot}} - \frac{1}{2} \rho_{\text{tot}} \hat{\sigma}_{he} \hat{\sigma}_{eh}]. \quad (12)$$

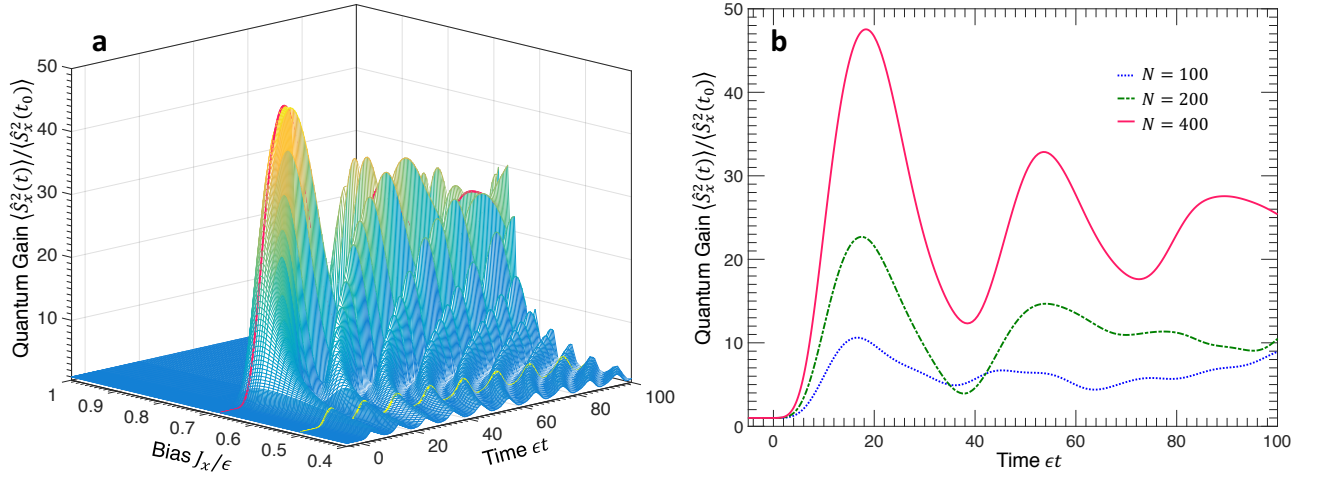


Figure 4. **Single-photon pulse induced first-order quantum phase transition.** **a** The quantum gain as a function of time and the bias spin-spin coupling J_x is shown. After absorption of a single-photon pulse, the absorber is flipped to the state $|e\rangle$, on which the absorber exerts a weak magnetic field $B_x \times P_e(t)$ ($P_e(t)$ the population of the state $|e\rangle$) on the amplifier with $N = 400$ spins. Only if the the amplifier is optically biased around the critical point $J_{x,c} \equiv J_y$, the time varying field can trigger a first-order quantum phase transition to obtain a large quantum gain. Here, the spin-spin coupling in y -direction is fixed at $J_y = 0.7\epsilon$ and the absorber-amplifier coupling $B_x = 0.01\epsilon$. **b** The time-dependent quantum gain $G(t)$ for different spin-number is shown. Here, the spin-spin couplings are $J_x = 0.675\epsilon$ and $J_y = 0.7\epsilon$.

We note that due to the dispersive coupling between the NV center and the amplifier, the dynamics of the absorber and the amplifier are almost "decoupled". After trace off the NV degree of freedom, the dynamics of the amplifier is given by

$$\frac{d}{dt}\rho_{\text{Am}}(t) = -i[\hat{H}'_{\text{Am}}, \rho], \quad (13)$$

where

$$\hat{H}'_{\text{Am}} = \hat{H}_{\text{Am}} + P_e(t)B_x \sum_j \hat{\sigma}_j^x, \quad (14)$$

and $P_e(t)$ is the population of the NV in the state $|e\rangle$. Here, we see that after transduction, the amplifier spins experience an effective magnetic field $P_e(t) \times B_x$ from the absorber. The dynamics of the absorber and the amplifier can be evaluated separately.

In Fig. 2, we give the time-dependent population (the net absorption probability) $P_e(t)$ of the state $|e\rangle$. The absorption probability P_e increases after the pulse arrives and finally reaches a steady-state value $P_{e,s}$. Here, the dissipation of the state back to $|g\rangle$ has been neglected due to the long life time of the metastate $|e\rangle$.

To realize an efficient single-photon transduction, we need to optimize the pulse length τ_f , the coupling strength Δ'' between the two excited states, and the two spontaneous decay rates γ_{fg} and γ_{he} . In experiment, we can use filters to tailor the pulse spectrum and change the pulse length [10]. The typical value of the coupling strength Δ'' is around 1 GHz. Usually, it is hard to tune this coupling strength. However, we can engineer the density of state of the electromagnetic fields to tune the decay rates γ_{fg} and γ_{he} [11–13] to enhance the transduction efficiency. In Fig. 3a, we show the optimization conditions for larger transduction probability. It has been shown that nearly unit transduction probability $P_{e,s}$ can be realized when $\gamma_{fg} = \gamma_{he} = \Gamma \gg 1/\tau_f$ for three-level atom system [14]. In Fig. 3b, we show that for four-level systems, unit probability $P_{e,s}$ can also be obtained when $\Gamma = 2\Delta'' \gg 1/\tau_f$.

In Fig. 4a, we show that only if the spiin-spin coupling J_x is biased close to the phase transition point $J_{x,c} = J_y$, a large quantum gain can be obtained. The red curve and the yellow curve correspond to $J_x = 0.675\epsilon$ and $J_x = 0.5\epsilon$, respectively. In Fig. 4b, we show that time T_{Am} to reach the maximum of the quantum gain is almost independent on the spin number N . However, the quantum gain increases with N linearly, which is consistent with our previous result [15]

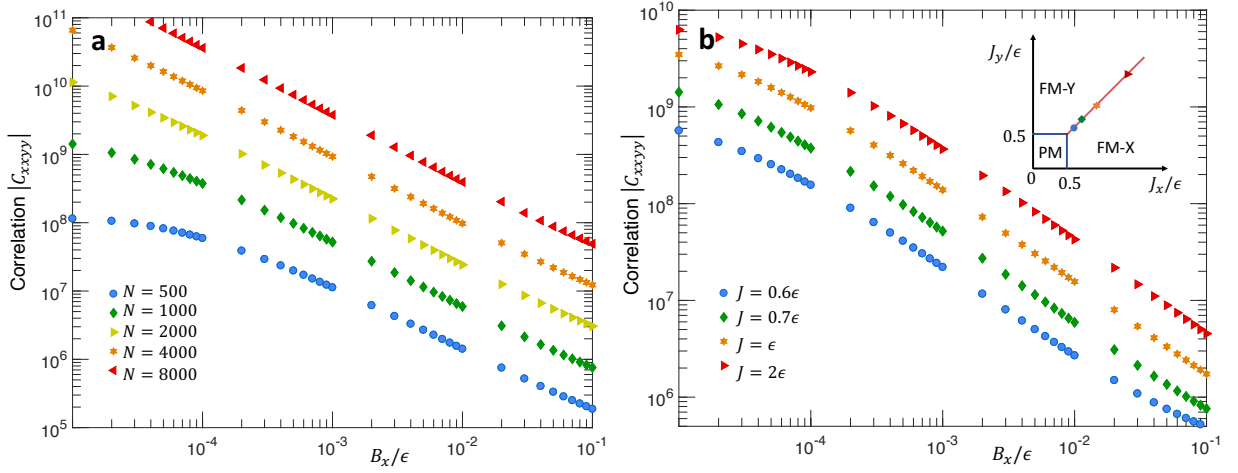


Figure 5. **Universal singular exponent.** **a** The correlation functions C_{xxyy} for different spin number N are shown. Here, the spin-spin coupling is fixed at $J_x = J_y = 0.7/\epsilon$. **b** The correlation functions C_{xxyy} for different spin-spin coupling strength $J_x = J_y = J$ are shown. The subgraph shows the corresponding positions on the phase diagram for different J . Here, the spin number is fixed at $N = 1000$. The singular scaling $C_{xxyy} \propto |B_x|^{-\gamma}$ does not change with spin number N as well as J .

III. HIGHER-ORDER CORRELATION

In thermodynamic phase transitions, the divergences of the magnetic susceptibility and spatial correlation length are directly related. The Gibbs partition function in a magnetic field h is given by [17]

$$Z = \text{Tr} \exp(-\beta \hat{H}_0 + \beta h_\alpha \hat{M}_\alpha), \quad (15)$$

where \hat{H}_0 describes the internal energy of the magnet including spin-spin interactions and $-h_\alpha \hat{M}_\alpha$ is the work done against the magnetic field to produce a magnetization $\langle \hat{M}_\alpha \rangle$ in the direction $\alpha = x, y, \text{ or } z$. The equilibrium magnetization is computed from

$$\langle \hat{M}_\alpha \rangle = \frac{\partial \ln Z}{\partial \beta h_\alpha} = \frac{1}{Z} \text{Tr}[\hat{M}_\alpha \exp(-\beta \hat{H}_0 + \beta h_\alpha \hat{M}_\alpha)], \quad (16)$$

and the susceptibility is then related to the variance of the magnetization by

$$\chi_\alpha = \frac{\partial \langle \hat{M}_\alpha \rangle}{\partial h_\alpha} = \beta \left\{ \frac{1}{Z} \text{Tr}[\hat{M}_\alpha^2 \exp(-\beta \hat{H}_0 + \beta h_\alpha \hat{M}_\alpha)] - \frac{1}{Z^2} \text{Tr}[\hat{M}_\alpha \exp(-\beta \hat{H}_0 + \beta h_\alpha \hat{M}_\alpha)]^2 \right\} \quad (17)$$

$$= \frac{1}{k_B T} \left(\langle \hat{M}_\alpha^2 \rangle - \langle \hat{M}_\alpha \rangle^2 \right). \quad (18)$$

The magnetization operator for discrete lattice systems is given by

$$\hat{M}_\alpha = \frac{1}{2} \sum_j \hat{\sigma}_j^\alpha, \quad (19)$$

for lattice system. Then, the relation between the susceptibility and the spatial correlation function is given by

$$\chi = \frac{1}{4k_B T} \sum_{ij} (\langle \hat{\sigma}_i^\alpha \hat{\sigma}_j^\alpha \rangle - \langle \hat{\sigma}_i^\alpha \rangle \langle \hat{\sigma}_j^\alpha \rangle) \equiv \frac{1}{k_B T} C_{\alpha\alpha}. \quad (20)$$

Utilizing the translational symmetry of a homogeneous system, we can connect the bulk response function with the microscopic two point correlation functions,

$$C_{\alpha\alpha} = \frac{N}{4} \sum_j \langle [\hat{\sigma}_j^\alpha - \langle \hat{\sigma}_j^\alpha \rangle][\hat{\sigma}_1^\alpha - \langle \hat{\sigma}_1^\alpha \rangle] \rangle \equiv \frac{N}{4} \sum_j G_{1j}^{\alpha\alpha}. \quad (21)$$

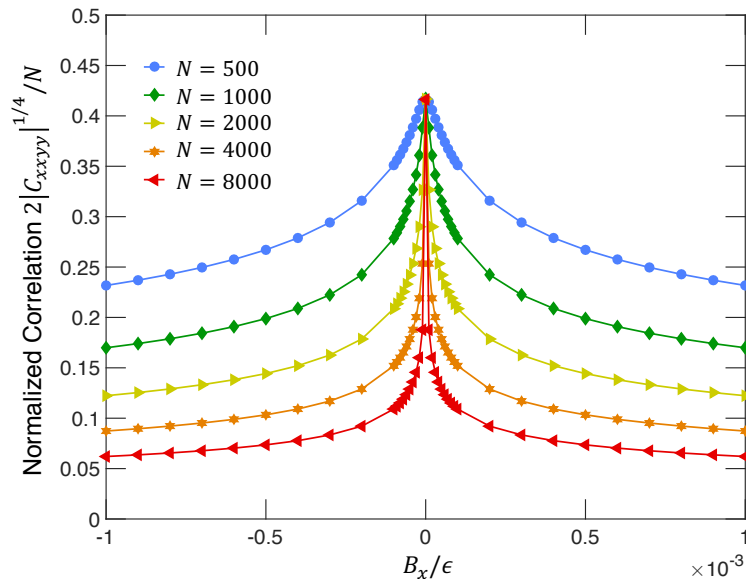


Figure 6. **Re-scaled correlation function.** Different curves denote different spin number. Here, the spin-spin coupling is fixed at $J_x = J_y = 0.7/\epsilon$.

In many cases, the correlation function decays as $G_{1j}^{\alpha\alpha} \propto \exp(-|j-1|/\xi)$ at separations $|j-1| > \xi$. Here, ξ called the correlation length is the only relevant length at the phase transition point.

However, at the first-order quantum phase transition (QPT) points, the singular behaviors occur on the correlation between the magnetic fluctuations in x and y directions. It can be easily verified that the lowest-order symmetrized macroscopic correlation function

$$C_{xy} = \frac{1}{2} \langle \hat{S}_x \hat{S}_y + \hat{S}_y \hat{S}_x \rangle - \langle \hat{S}_x \rangle \langle \hat{S}_y \rangle, \quad (22)$$

due to the symmetry of the spontaneous magnetization in xy -plane. Here, $\hat{S}_\alpha = \sum_i \hat{\sigma}_i^\alpha / 2$ is the collective angular momentum operator. Thus, we need to consider the higher-order correlation

$$C_{xxyy} = \frac{1}{2} \langle \hat{S}_x^2 \hat{S}_y^2 + \hat{S}_y^2 \hat{S}_x^2 \rangle - \langle \hat{S}_x^2 \rangle \langle \hat{S}_y^2 \rangle. \quad (23)$$

The singular scaling of C_{xxyy} has been shown in Fig. 4 (a) in the main text. Here, we show that this scaling is independent on the spin number and the position on the phase transition boundary. In Fig. 5a, we contrast the correlation C_{xxyy} with different spin number. In Fig. 5b, we contrast the correlation C_{xxyy} with different spin-spin coupling $J_x = J_y = J$. We see that the value of C_{xxyy} changes, but the scaling exponent γ of $C_{xxyy} \propto |B_x|^{-\gamma}$ at the phase transition point remains the same.

As explained in the main text, we can not define a simple correlation length ξ for the LMG model with indistinguishable spins. However, we may use the rescaled correlation function

$$\eta = \frac{2}{N} |C_{xxyy}|^{1/4}, \quad (24)$$

to characterize the proportion of correlated spins. As shown in Fig. 6, the size of correlated spin clusters decreases away from the phase transition point.

-
- [1] Y. Chu, M. Markham, D. J. Twitchen, and M. D. Lukin, *Phys. Rev. A* **91**, 021801 (2015).
 [2] J. R. Maze, A. Gali, E. Togan, Y. Chu, A. Trifonov, E. Kaxiras, and M. D. Lukin, *New Journal of Physics* **13**, 025025 (2011).
 [3] L.-P. Yang, H. X. Tang, and Z. Jacob, *Phys. Rev. A* **97**, 013833 (2018).

- [4] E. Togan, Y. Chu, A. Trifonov, L. Jiang, J. Maze, L. Childress, M. G. Dutt, A. S. Sørensen, P. Hemmer, A. S. Zibrov, *et al.*, *Nature* **466**, 730 (2010).
- [5] L.-P. Yang, C. Khandekar, T. Li, and Z. Jacob, *arXiv preprint arXiv:1904.02796* (2019).
- [6] B. Q. Baragiola, R. L. Cook, A. M. Brańczyk, and J. Combes, *Phys. Rev. A* **86**, 013811 (2012).
- [7] H. J. Lipkin, N. Meshkov, and A. Glick, *Nuclear Physics* **62**, 188 (1965).
- [8] N. Meshkov, A. Glick, and H. Lipkin, *Nuclear Physics* **62**, 199 (1965).
- [9] A. Glick, H. Lipkin, and N. Meshkov, *Nuclear Physics* **62**, 211 (1965).
- [10] A. M. Weiner, *Progress in Quantum Electronics* **19**, 161 (1995).
- [11] E. M. Purcell, H. C. Torrey, and R. V. Pound, *Phys. Rev.* **69**, 37 (1946).
- [12] D. Kleppner, *Phys. Rev. Lett.* **47**, 233 (1981).
- [13] E. Yablonovitch, *Phys. Rev. Lett.* **58**, 2059 (1987).
- [14] S. M. Young, M. Sarovar, and F. m. c. Léonard, *Phys. Rev. A* **97**, 033836 (2018).
- [15] L.-P. Yang and Z. Jacob, *Optics express* **27**, 10482 (2019).
- [16] L.-P. Yang and Z. Jacob, *arXiv preprint arXiv:1905.07420* (2019).
- [17] M. Kardar, *Statistical physics of fields* (Cambridge University Press, 2007) , Chap. 1.